The Quartz Crystal Microbalance as a Continuous Monitoring Tool for the Study of Endothelial Cell Surface Attachment and Growth

ARTICLE *in* BIOTECHNOLOGY PROGRESS · DECEMBER 1999

Impact Factor: 2.15 · DOI: 10.1021/bp000003f · Source: PubMed

5 AUTHORS, INCLUDING:

Tiean Zhou
Hunan Agricultural University
16 PUBLICATIONS **533** CITATIONS
SEE PROFILE

Susan J Braunhut
University of Massachusetts Lowell
45 PUBLICATIONS **1,450** CITATIONS
SEE PROFILE

The Quartz Crystal Microbalance as a Continuous Monitoring Tool for the Study of Endothelial Cell Surface Attachment and Growth

Tiean Zhou,[†] Kenneth A. Marx,*[,†] Michael Warren,[‡] Heather Schulze,[‡] and Susan J. Braunhut[‡]

Center for Intelligent Biomaterials and Departments of Chemistry and Biological Sciences, University of Massachusetts, Lowell, Massachusetts 01854

The quartz crystal microbalance (QCM) was used to monitor endothelial cell (EC) adhesion on the gold surface of an oscillating quartz crystal contained in a QCM device. A number of parameters were investigated. First, we observed differential QCM O-ring toxicities for ECs. Second, appropriate conditions for cell culture and QCM cell environment were identified that can eliminate large-scale frequency oscillations in the measurements. These artifacts are not due to added cells but originate in the time-dependent evaporation of water. Having eliminated these artifacts, we then demonstrated that the measured steady-state crystal frequency shift, Δf, and motional resistance shift, ΔR, were determined by the number of firmly attached ECs requiring trypsinization from the crystal surface. Last, following steady-state attachment of ECs, the EC growth stimulation by fibroblast growth factor was monitored in a continuous fashion by measuring f and R values over a 72 h. period. We observed the Δf values to increase in a way that reflected the increase in EC number bound to the QCM surface. Following addition of ECs to the QCM, the time-dependent increase in ΔR can be interpreted in terms of increase by the ECs of the energy dissipation properties of the solution at the solution−gold surface interface. This effect is due to their rapid surface attachment and the elaboration of their cytoskeletal properties. These results indicate that the QCM technique can be used for the study of EC attachment and growth and suggest its potential for the real time study of per unit surface area cell mass distribution dynamics and viscoelastic properties and the cells' responses to stresses or perturbations brought about using biologically active molecules.

Introduction

The elastic mass and viscoelastic behavior of surface-bound materials can be sensitively detected and distinguished at the gold−solution interface above a piezoelectric quartz crystal oscillating in a quartz crystal microbalance (QCM). The QCM was applied initially to measurement of the mass binding to the quartz surface from chemical species in the gas phase. More recently, the solution-based QCM has been developed as a tool in analytical electrochemistry. The elastic mass added to the QCM surface can be precisely quantified through changes in frequency, f, using the Sauerbray equation, with a ng detection sensitivity (*1*). It is capable of sensitively measuring mass changes associated with liquid−solid interfacial phenomena, particularly at electrodes (*2*−*5*). Viscosity−density solution effects on the crystal f and resistance, R, values can be distinguished from surface-bound elastic mass shifts using established techniques (*6*−*8*).

With the development of aqueous solution QCM techniques, biosensors have been created in which biological macromolecules have been incorporated into the sensing system design (*9*−*22*). Going a step further, whole cells can be monitored when they are bound to the QCM surface. A number of surface-adherent cell types have been examined, including osteoblasts, human platelets, MDCK I and II cells, 3T3 cells, VERO cells, CHO and MKE epithelial cells, and microbial biofilms (*23*−*30*). Notwithstanding considerable variability in reported results, these studies all serve to establish the basic principle, which is that adherent cells cause a reversible QCM frequency shift. The magnitude of this frequency shift does not obey the simple Sauerbray equation, which only quantitates bound elastic mass that dissipates no energy. However, little has been done to use the sensitive quantitative capabilities of the QCM to correlate measured f and R values with bound cell type, their number, or properties or to investigate the behavior of adherent cells in response to chemical, biological, or physical changes in their environment.

Endothelial cells (ECs) represent an important cell type in the body. They line the blood vessels by forming a continuous monolayer of cells (*31*). In large vessels closest to the heart, the EC monolayer resides upon a basement membrane shared by multiple layers of smooth muscle cells (*32*). ECs rarely proliferate in vivo, allowing them to be involved in the regulation of vessel diameter, blood flow, and the movement of gases, nutrients, and metabolic waste between the plasma and interstitial spaces (*33*). ECs are tightly growth regulated and, in

* Ph: (978) 934-3658. Fax: (978) 934-3013. Email: Kenneth_Marx@uml.edu.
[†] Center for Intelligent Biomaterials and Department of Chemistry.
[‡] Department of Biological Sciences.

10.1021/bp000003f CCC: $19.00
Published on Web 03/02/2000

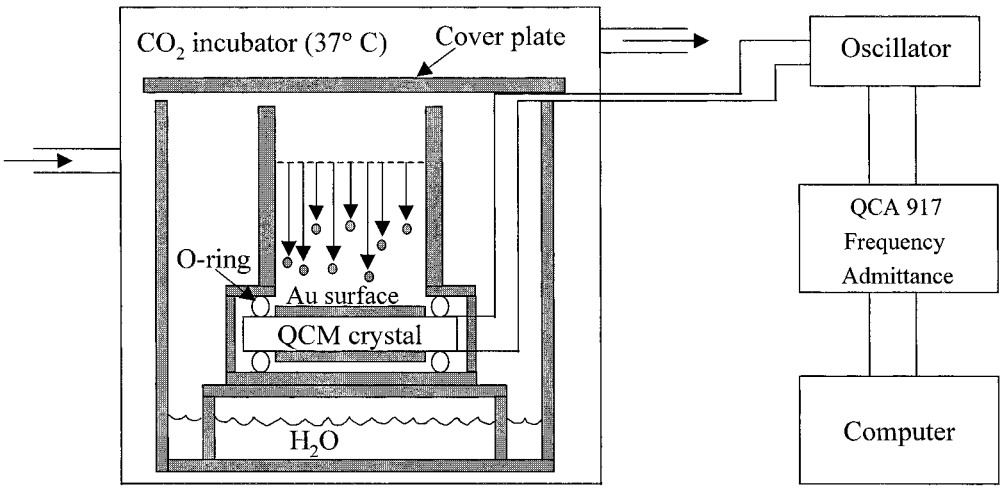

Figure 1. Schematic of the QCM measurement system.

some tissues, have been estimated to divide only once every 3 years (*34*).

During wound healing or in association with particular pathologies, angiogenic signals can rapidly stimulate ECs of postcapillary venules to become mobilized from these otherwise established vessels and to proliferate (*35*). During this change from a nongrowing to a growing, migratory state, the endothelium is required to alter its cell shape and its binding to the underlying extracellular matrix (ECM). ECs are associated with the matrix via coupling of cytoskeletal elements to the plasma membrane at inner cytoplasmic domains termed focal adhesion complexes and integrin receptors that span the plasma membrane (*36*). Focal adhesion complexes and integrin receptors possess extracellular domains that can in turn bind directly to sequences found within the ECM molecules (*37*). Little is known about the mass redistribution ECs engage in when changing from a dividing, poorly adherent cell to an adherent, nondividing cell.

In a preliminary study, we have described the time-dependent sequence of initial contact, immediate adhesion, and spreading of normal bovine ECs as they sediment to, contact, and spread on the QCM surface (*38*). In this report, we study a number of parameters affecting cell monitoring with the QCM technique. These include varying O-ring toxicity for ECs and an observed long-range frequency oscillation artifact, due to water evaporation, which was eliminated via modification of the experimental setup. Of major importance, we demonstrate the necessity of relating the QCM Δf and ΔR crystal shifts to the cell number bound, as determined by electronic counting of the cell number requiring trypsinization from the gold QCM surface at the conclusion of the experiment rather than the number of cells added to the QCM cell. We also demonstrate that growth stimulation of ECs by fibroblast growth factor (FGF) on the QCM surface results in a Δf shift that reflects the increase in cell number bound to the QCM surface. Last, we demonstrate that from the first few minutes ECs bind to the gold QCM surface through their establishment of a stable attached steady state at 24 h, a dramatic increase occurs in the energy dissipation properties of the QCM solution−surface interface, going from an initial pure liquidlike viscoelastic behavior to a state of greater energy dissipation.

Materials and Methods

Quartz Crystal Microbalance for Cell Adhesion. An AT cut quartz crystal of resonant frequency 8.85 MHz with gold electrode (5 mm diameter) was used in a cylindrical Teflon cell. AT cut crystals are the standard commercial QCM crystals available (Seiko EG&G) and result from preparation via specific (yxl) 35° 15′ oriented cuts of the quartz substrate. An advantage of the AT cut crystal is that their f values are relatively invariant to temperature changes. The crystal was sandwiched between two O-rings to allow only one side of the electrode to be exposed to the media- and serum-containing solution (Figure 1). The QCM device was placed within a large Petri dish filled with distilled water. The QCM crystal in its well holder was placed on an inverted glass Petri dish at a level well above the water surface. This 37 °C water reservoir allowed humidity to be maintained, preventing evaporation from the QCM cell. Also, to prevent evaporation, the QCM was covered with a Petri dish cover plate following placement inside a temperature-regulated cell incubator. A model QCA 917 quartz crystal analyzer system (Seiko EG&G), comprising a main unit and an oscillator, was used for the simultaneous measurement of the resonant frequency (f) and resonance admittance (A). After sterilization with ethanol (0.5 h) and washing with water and PBS, 52 μL of defined Dulbecco's Minimal Eagle's Medium (DMEM) with 10% calf serum (CS) was added onto the QCM electrode, and the entire holder, in the crystallization dish, was put into a humidified CO_2 incubator controlled at 10% CO_2 and 37° C and covered. The QCM electrodes were wire extended to the oscillator driven by the main unit of the QCA 917. The f and A (from which R is calculated) values were automatically monitored at 1 min intervals using a PC and WinWedge 32, version 3.0 Software (TAL Technologies), and the stable values at 2 h were taken as reference values before the addition of cells. At 2 h, 250 μL of DMEM−10% CS containing a specific number of cells was added evenly to the medium surface. The ECs attached to the QCM surface following sedimentation through the overlaying 0.68 cm depth (302 μL) of medium and serum (see Figure 1). Then, f and A values were automatically monitored during the process of cellular sedimentation to the crystal surface and during their impact and spreading over several hours to several days. Values of A, in μS were converted into motional resistance, R, in units of Ω, using the relationship $R = 10^6/A$.

Cell Culture, Cell Attachment to the QCM, and Removal via Trypsinization. Bovine aortic endothelial cells (BAEs) were originally obtained from Ms. Sandie Smith and Dr. Patricia D'Amore at the Children's Hospital, Boston, MA and were maintained as stock cultures

in DMEM−10% CS, as previously described by us (*39*). BAEs were not used beyond passage 22. For experimental treatments, ECs were trypsinized and washed with PBS, and precise counts of the number of cells were made using an electronic cell counter (Coulter, Inc.) following resuspension in full media (250 μL). At the end of a QCM experiment, cells firmly attached were determined via trypsinization assay and an electronic counter. This protocol involved the following steps. Media was collected from the QCM (M). The QCM was gently washed with 100 μL of PBS (W). After 125 μL of trypsin (0.05% w/v trypsin, 0.53 mM EDTA, in Hank's buffered salt solution) was added and incubated for 6 min at 37 °C, this fraction was collected (T_1). Following a second trypsinization wash, identical to the first, this fraction was collected (T_2). Aliquots from all of the four wash steps were electronically counted using Coulter counting. After trypsinization, the QCM electrode was washed successively with PBS, water, and ethanol and then detached from the well holder. It was then cleaned sequentially with 4 M guanidine·HCl (1 h), 8 M guanidine·HCl (0.5 h), 1 M NaOH (0.5 h), and 1 M HCl (25 min), rinsed with water and ethanol, and then dried under nitrogen flow. Cleaned in this way, to remove all residual ECM and cell debris, the QCM was used repeatedly with good reproducibility of its initial frequency value due to complete protein removal from the QCM surface.

For O-ring toxicity studies, the cells were first grown to confluency in 35 mm Petri dishes. The individual 0-rings (size, DASH 009, McMaster-Carr Supply Co.) were then added to the dishes and were of three different types: Viton, ethylene propylene, and silicone. Following a 48−72 h interval, cells in the culture dish surface area adjacent to the O-ring were photographed under phase illumination microscopy. In the FGF experiments, a 3 ng/mL final concentration was used to stimulate the EC.

Results

Cellular Origin of Δf and ΔR Shifts and Elimination of Evaporation-Based Δf and ΔR Oscillation Artifacts. A cross section schematic view of the experimental QCM measurement system is depicted in Figure 1. Added cells are indicated sedimenting (vertical arrows) through the media and serum contained within the cylindrical QCM cell holder to the gold surface on the upper face of the QCM crystal. This quartz crystal oscillates initially at its resonance frequency of 8.85 MHz. As the cells contact the surface and adhere, they cause a decrease in the f values and an increase in the R values of the oscillating QCM crystal.

In Figure 2A, we illustrate how Δf and ΔR vary with time following the addition of cells to the QCM device. The time dependence of both f and R values are presented as Δf and ΔR values relative to 0, which corresponds to the f and R values of the crystal immediately preceding addition of the ECs and reflects baseline values with media. In this experiment, 20 000 cells were added to the QCM device at the point shown by the arrowhead. Initially, f decreases and R increases steadily, reaching their maximum shifted values simultaneously around 45 min after cell addition. These early maximum Δf and ΔR shift values we hypothesize are due to the rounded cells contacting the gold QCM surface and initiating attachment. As the cells spread on the surface and elaborate their attachment to the underlying substrate, the f and R values moderate and reach steady-state Δf and ΔR shifted values after 20−24 h.

In all of our early cell experiments in the QCM device, we observed a sinusoidal type of oscillation in both the

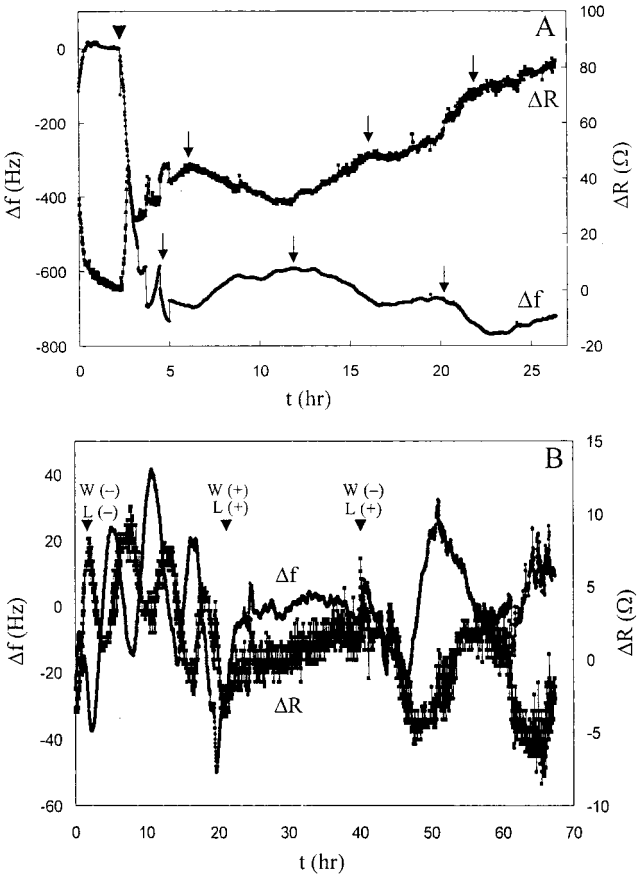

Figure 2. QCM recorded Δf and ΔR values as a function of time following (A) addition of 20 000 cells (at arrowhead), oscillation in Δf and ΔR is indicated by the small vertical arrows at successive peak maxima; (B) a series of environment modifications of the QCM cell containing PBS but no added cells. The arrowheads indicate the following different environments: W(−), L(−) means no water reservoir in the Petri dish holding the QCM cell and no Petri dish lid; W(+), L(+) means a water reservoir was present and a Petri dish lid was on the Petri dish; W(−), L(+) means no water reservoir was present, but a lid was covering the Petri dish holding the QCM cell.

Δf and ΔR values over time intervals of hours. This behavior, with a period of from 5 to 10 h, is clear for both Δf and ΔR (arrows indicate peak maxima) in Figure 2A, even under steady-state conditions. This oscillation is not due to the behavior of cells but to water evaporation as we demonstrate in Figure 2B. When a water reservoir is placed beneath the QCM cell (W+) and a lid (L+) is placed over the Petri dish containing the QCM well holder (second arrowhead), thereby preventing evaporation, the oscillation is totally eliminated. For two other experimental conditions where evaporation can occur, L(+), W(−) at a slower rate and L(−), W(−) at a faster rate, we observed oscillations of 15 h and 5 h respectively, in good agreement with the evaporation origin of this artifact. We eliminated this oscillatory artifact in all subsequent experiments by modifying the system with the QCM cell placed on a pedestal immediately above a reservoir of temperature-equilibrated water, inside a covered large Petri dish, inside the humidified incubator as shown in Figure 1. This is the configuration used for the W(+), L(+) experimental condition in Figure 2B. The Petri dish plate remained covering the QCM at all times except during the addition of cells and during cell counting at the conclusion of the experiment.

O-Ring Variability and Cell Toxicity. Another troublesome initial feature of the QCM monitoring of

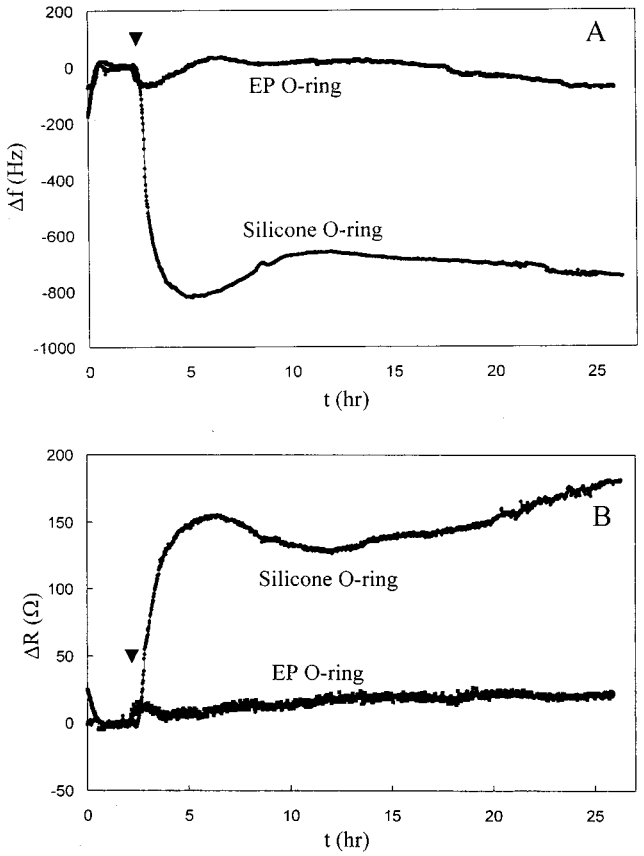

Figure 3. QCM O-ring dependence of (A) Δf values and (B) ΔR values, as a function of time following addition of 20 000 cells (at arrowheads) to the QCM device containing either a silicone O-ring (biocompatible) or an EP O-ring (toxic).

added cells was the variable cell response to the type of O-ring used to seal the cell about the QCM crystal (see Figure 1). The upper O-ring, contacting the media and serum, affected the cells on the gold QCM surface. Figure 3A and B, respectively, show Δf and ΔR values recorded in response to 20 000 added cells using two types of O-rings. The responses are clearly different for these two O-rings. Cells exposed to the silicone O-ring achieved significant steady-state Δf (−740 Hz) and ΔR (180 Ω) shift values, indicative of healthy cell behavior as we observed in Figure 2A. However, cells in the presence of the ethylene/propylene (EP) O-ring showed a greatly diminished steady-state Δf and ΔR shift response, close to 0, indicative of poor cellular mass attachment to the gold QCM surface.

To independently demonstrate the effect of the different O-rings upon cells, we carried out experiments in which confluent monolayers of endothelial cells were prepared in a series of Petri dishes in which three different O-rings were placed, one to a dish. Following 48 h in culture, the cells in the vicinity of the O-rings were photographed using phase microscopy. These results are presented in Figure 4. Panel A shows a representative field of healthy cells from a control plated dish not containing any O-ring. In panels B and C, healthy cells are shown growing normally in the vicinity of, respectively, Viton and silicone O-rings (biocompatible), which appear as dark shadow areas at the top of each image. By contrast, in panel D, in the presence of the EP O-ring (toxic), few cells appear healthy and well spread and most appear rounded and in stress. Some cells appear to be dead and floating. These results agree with the QCM Δf and ΔR results already presented for the silicone and EP O-rings in Figure 3A and B. That the origin of this deleterious O-ring effect on cells is due to a diffusible factor coming from the EP O-ring is confirmed by the result in panel E. In this Petri dish, cells in culture with an extensively prewashed EP O-ring are shown. This EP O-ring, with prior demonstrated toxicity, had been washed by storage in PBS solution for 14 days, with several changes of PBS. After this extensive washing, the O-ring was re-added to cells. Clearly, in this case, the cells appear normal and in reasonable numbers. We interpret this result to mean that the lengthy PBS pretreatment removed most or all of the diffusible factor that was responsible for the deleterious results observed in panel D and in Figure 3. As a result of these experiments, in all subsequent experiments we used the biocompatible silicone O-ring from McMaster-Carr, Inc.

Long-Term Cell Growth Monitoring with QCM Requires Trypsinization and Counting To Prove Cell Attachment. The utility of the QCM as a cell biologist's tool for the study of cells requires that the technique meet certain criteria. Preferably, the QCM must be capable of monitoring cell behavior over several cell cycle divisions. The relationship between the measured QCM f and R values must be clearly relatable to both the number of cells and the behavior of those cells. The latter relationship is not the primary focus in this report. Understanding that relationship will require extensive experimentation to relate QCM parameters to both the structure and dynamics of the complex molecular machinery in the cellular interior and also to the integrin receptors at its periphery involved in adhesion to the QCM surface. In this report, however, we will first show the importance of demonstrating the exact number of attached cells responsible for the measured QCM Δf and ΔR shift responses, via a double trypsin assay.

We carried out the following experiment to establish the number of cells actually adhering to the QCM surface and which are therefore responsible for the observed Δf and ΔR values at the termination of an experiment. Following addition of 20 000 cells to the QCM, the f and R values were automatically recorded at 1 min intervals out to the 24 h steady-state condition. In Figure 5, we show the invariant steady-state 24 h Δf and ΔR values. Before addition of cells at time 0, the Δf and ΔR values were 0, representing the properties of the clean gold QCM surface, preequilibrated with media and serum. Thus, steady-state Δf and ΔR values after cell addition represent, potentially, the adherent cells as well as the underlying extracellular matrix (ECM) they have deposited. To demonstrate that the shifted Δf and ΔR values representing the steady state are due to only firmly bound cells and ECM, we performed trypsinization while continuing QCM measurements. This was monitored in two ways, via electronic cell counting of washes of the gold crystal surface and via the QCM measurements directly following each of the washes.

As is clear from Figure 5, only when the first trypsin incubation was initiated did the f and R values begin to change significantly. Rapidly, in the minute before the first measurement could be recorded, the Δf and ΔR values had begun to change significantly. Within 3−5 min, both Δf and ΔR reach 0, their original 0-time values. Following the second trypsin incubation, the ΔR value remains at 0 and the Δf value is nearly unchanged, rising slightly above 0. Following removal of the second trypsin wash, media with serum at 37 °C was added to the QCM. The ΔR value remained at 0, and the Δf value was observed to be restored to 0, both being the values measured for the original gold surface preequilibrated

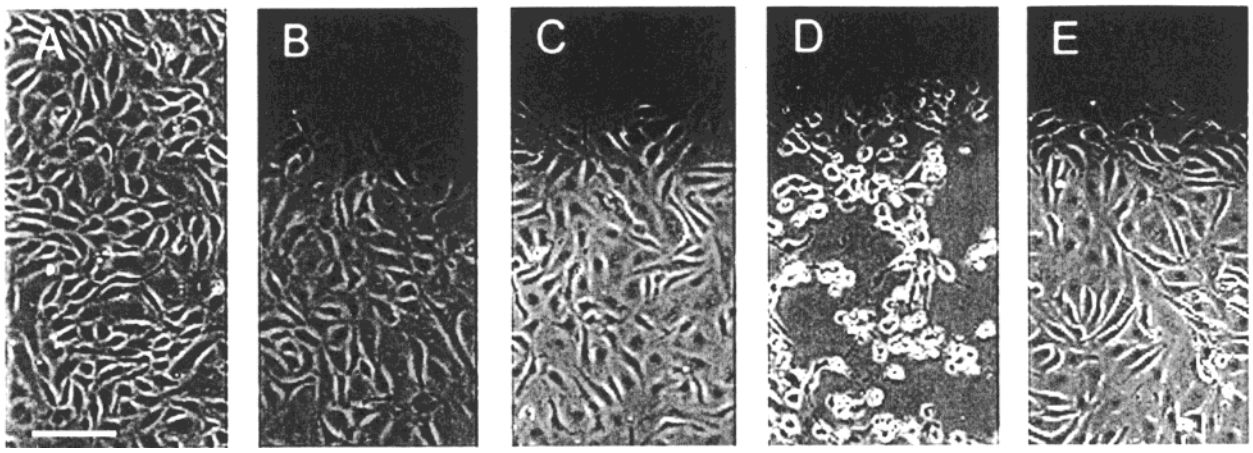

Figure 4. Phase contrast photomicrographs of ECs in a series of culture dishes: (A) control cell dish; (B) cells grown in the presence of a Viton O-ring (biocompatible); (C) cells grown in the presence of a silicone O-ring (biocompatible); (D) cells grown in the presence of an EP O-ring (toxic); (E) cells grown in the presence of a long-term (14 days) PBS-washed EP O-ring.

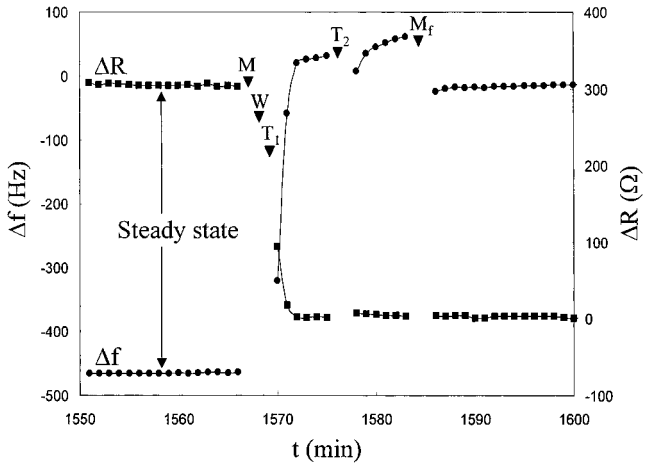

Figure 5. Trypsinization kinetics recovery of pre-addition QCM Δf (●) and ΔR (■) values from an established steady-state cell population (20 200 total trysin counted cells at 24 h) adhering to the gold QCM surface. Initially, 30 000 cells were added to the QCM surface. Arrowheads indicate the time of the four washes and the final assay condition: M, media and serum from the experiment; W, the PBS wash; T_1, the first trypsin digest; T_2, the second trypsin digest; M_f, the final media and serum incubation to determine the gold surface state.

with media and serum, before addition of ECs. Trypsinization is a standard method for detaching adherent cells from tissue culture plates, via cleavage of the outer plasma membrane domains of integral membrane proteins including integrins, the receptors that bind cells to ECM and via cleavage of ECM proteins on the QCM surface. Therefore, the recovery of the original 0-time QCM f and R values must be as a result of total resuspension and detachment of the adherent cells and their underlying ECM.

To prove that the QCM steady-state Δf and ΔR values were produced by removing firmly attached cells from the QCM surface via the multistep trypsinization protocol, we saved the four solutions, media and serum removed, PBS wash, trypsin 1, and trypsin 2, and performed electronic cell counting on each of them. The total cell numbers observed in each wash are presented in Table 1 for four different initial cell loadings, along with their steady-state Δf and ΔR values, measured using the biocompatible silicone O-ring. At the conclusion of all four experiments, we observe that the majority of added cells are found in the first of two trypsin incubation solutions. This is consistent with the observations we presented in Figure 5 that Δf and ΔR shift values do not change significantly until the first trypsin incubation. Then, nearly the entire change in shift values, back to their pre-cell-addition values, is accomplished with the first trypsin incubation. The Table 1 results agree with the Figure 5 results in two other ways. First, Table 1 shows that the largest fraction of cells removed by trypsinization are found in the first trypsin incubation. Second, the % of total recovered cells represented by the trypsin incubation fractions is nearly consistently over 80%. We believe that the number of cells found in the media and serum reflect cell fragments or cells that have previously detached. Cells detected in the PBS wash most likely represent mitotic or loosely bound unhealthy cells. The range of numbers observed for % recovery of added cells is in agreement with findings using conventional cell culture plasticware, in that a plating efficiency of about 70−80% for ECs is observed at each passage.

The final row in Table 1 reports the cell counting results from the Figure 3 experiment using 20 000 cells with the toxic EP O-ring. Clearly, there is a greater percentage of cells in the media and PBS than in the trypsin washes when compared to the experiment with the biocompatible silicone O-ring in which the same number of cells (20 000) were added to the QCM. Furthermore, only 20−23% of the total cells were recovered using the toxic O-ring. Only when there exist significant numbers of cells, requiring trypsin to be removed from the QCM surface, do we observe significant Δf and ΔR shifts.

It is clear from Table 1 that healthy cells cause significant steady-state shifts of −470 to −620 Hz for Δf and 200−300 Ω for ΔR, while unhealthy unattached cells cause minor shifts, as was the case when using the EP O-ring. However, there appears to be no clear relationship between the steady-state Δf, ΔR QCM shift values, and either the number of added cells or the number of attached cells demonstrated by the trysin assay.

Continuous Long-Term Monitoring of EC Growth Stimulation with FGF. To demonstrate the ability of the QCM to monitor cells in real time over extended intervals as the cells undergo a significant biological change, we carried out the experiment shown in Figure 6. Here 7 500 added ECs are being stimulated (at FGF arrowhead) with 3 ng/mL FGF, 24 h after loading into the QCM cell (at left arrowhead) and after having established their characteristic adherent steady-state shift values. From the time of FGF stimulation, the Δf is observed to drop steadily for approximately the next

Table 1. QCM Parameters and Total Cell Counts from a Series of Washes of the QCM Surface, 24 h after Cell Addition

	washes (cells recovered)				cells in trypsin washes		QCM*	
cells added	media + serum	PBS	trysin 1	trypsin 2	% of added	% recov	Δf (Hz)	ΔR (Ω)
				Silicone O-ring (biocompatible)				
10 000	2 460	1 630	5 780	730	65	61	−520	200
20 000	1 200	870	12 480	5 050	88	89	−620	275
30 000	3 510	1 350	17 730	2 490	67	81	−470	300
50 000	3 240	1 240	31 160	2 040	66	88	−570	300
				EP O-ring (toxic)				
20 000	6 290	2 130	2 980	1 630	23	20	−70	20

*Both Δf and ΔR values represent steady-state values at 24 h following cell addition.

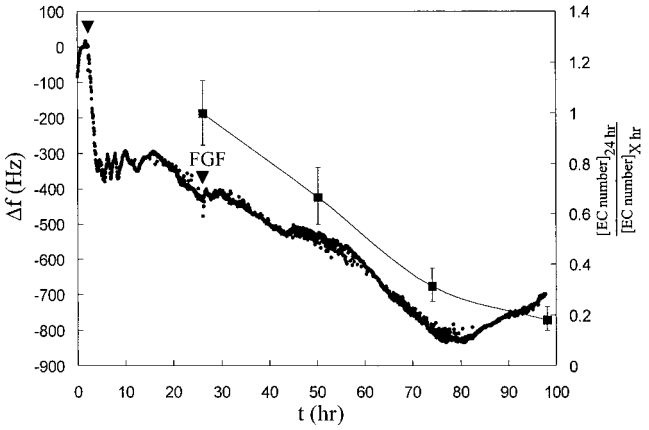

Figure 6. Long-term recorded QCM Δf and ΔR values during an FGF stimulation experiment with 7 500 added cells. ECs were placed on the crystal surface (first arrowhead) and after achieving steady state, 3 ng/mL FGF was added (second arrowhead). The four washes were carried out at the conclusion of the experiment. The right-hand axis displays the results of a parallel tissue culture experiment involving identical FGF stimulation of a similar population of ECs in multichamber well plates. The data are displayed as the ratio of initial averaged triplicate electronic countings of ECs at 24 h divided by the averaged triplicate electronic countings of FGF stimulated ECs at the indicated time points.

55 h, from −400 to −830 Hz. At around 80 h, the Δf shift reverses direction and begins to rise steadily for the remainder of the experiment. The 55 h during which Δf drops corresponds to about two cell cycles. Since 7 500 ECs were loaded into the QCM, and if our plating efficiency was around 65−70% as Table 1 suggests, then 4 875 ECs would have firmly attached to the QCM surface as viable cells. At the conclusion of the FGF stimulation experiment, we counted the cells and found 15 490 ECs in the two trypsin washes of the QCM surface. This cell count represents an estimated 3.0−3.2-fold EC growth on the QCM surface, or nearly 2 cell doublings, during the nearly two cell cycle length experiment in which the Δf was observed to drop.

To ascertain the effect of 3 ng/mL FGF on these ECs in conventional tissue culture plasticware, we carried out a separate experiment using a portion of the same starting cell population that was used in the QCM experiment. These ECs were plated into multichamber 48-well plates, at a similar density to that used in the QCM experiment. Following 3 ng/mL FGF addition to one-half of the wells at 24 h, cells from triplicate wells were counted at the times indicated in Figure 6. We present the results of this parallel growth stimulation experiment as a ratio of the 24 h ECs count value divided by the FGF-stimulated ECs count value at the indicated times. Cell growth can be observed as a decrease in this ratio with time. From the data shown in Figure 6, the growth stimulation effect is dramatic and parallels the Δf shift nearly exactly over the course of the continuous Δf drop until 80 h. At this point, the cell growth stimulation effect of FGF has disappeared, and the growth is leveling off at the last time point. The change in growth state of the ECs must also be responsible for the reversal of the Δf shift at 80 h.

Discussion

QCM System Requirements: Preventing Evaporation and O-ring Testing To Eliminate Cell Toxicity. The oscillatory Δf and ΔR shift behavior we observed in initial QCM experiments in Figure 2A represents a phenomenon that has already been described theoretically and via experiment in the literature for QCM measurements of liquids (*40*−*42*). Due to a nonuniform surface velocity of liquid at the gold surface−liquid interface, a vertical liquid pressure wave is induced from the gold surface toward the surface of the liquid. Any change in the liquid column height can cause a change in the resonant frequency of the pressure wave since the dissipative standing shear waves emanating from the crystal surface are coupled to the liquid above it. When the net water evaporation from the solution corresponds to the loss of a lamella thickness of solution equivalent to one pressure wave wavelength (∼100 μm), the Δf and ΔR values will then have cycled through one complete oscillation because the total solution column length is now back in phase with the standing pressure waves in solution.

The Figure 2B result is in agreement with the origin of this oscillation being due solely to time-dependent water evaporation from the QCM cell. The oscillation period increased from about 5 to 15 h to effectively infinity as the evaporation went from its highest rate to a minimum when the system was modified to its final configuration, that presented in Figure 1. This system modification served two purposes. It effectively raised the water partial pressure in the atmosphere around the QCM to saturation at 37 °C, thereby minimizing any evaporation from the QCM cell. As it is designed to do, the Petri dish cover on the Petri dish reservoir allowed normal gas exchange with the incubator, thereby supporting long-term cell viability on the QCM surface.

We determined that the type of O-ring used in the assembled QCM cell can be critical for cell viability. The data in Figure 3A and B demonstrate that certain QCM O-rings, the EP type in our study, are toxic for the ECs we studied. The toxicity must result from some diffusible factor in the EP O-ring, which we showed through light microscopy in Figure 4 is toxic to ECs in culture dishes containing these O-rings. The toxic effect is expressed a considerable distance from the EP O-ring, as evidenced by the area adjacent to the EP O-ring being devoid of cells. This toxic effect is clearly due to a soluble factor because the O-ring floats and does not come into physical contact with the attached ECs. The other O-rings tested

had no clearing of cells adjacent to the O-rings. Extensive washing of EP O-rings, prior to incubation with the cells, resulted in removal or reduction of the diffusable factor, which rendered the washed O-ring biocompatible with the cells. Given that the EP O-ring is derived from processed polymers, the toxic species is likely to be either an unreacted monomer or a free radical initiator species. These experiments demonstrate that prior testing of O-rings by co-culture with the cells to be studied is necessary to eliminate the presence of potential toxic diffusible species during experiments.

QCM Response to Attached Cells: Δf and ΔR Shifts and Trypsin Cell Assay. A consistent observation in Figures 2A, 3A,B, and 6 and the experiments whose parameters are summarized in Table 1 is of an f decrease and R increase as the ECs contact the gold QCM surface and initiate attachment. We examined this phenomenon previously in a brief report, using a parallel experiment with ECs added to chambered LABTEK slides designed to exactly mimic the sedimentation distance of the ECs to the QCM device (*38*). We presented time-dependent phase microscopic evidence of the LABTEK surface that correlated the maximum f decrease and R increase at 45 min with the point at which all of the rounded cells hit and attached to the gold surface. Following the initial 45 min after cell addition, f increased and R decreased from their maxima, proceeding to their steady-state values, as we have described in this report. At the 24 h steady-state condition, the micrographs clearly showed that normal ECs extend processes and undergo a familiar anchorage-dependent process known in vitro to involve laying down of ECM, to which the cells attach via integral membrane protein receptors composed of integrins. Thus, we have a reasonable qualitative understanding of the cell behaviors related to cell contact and attachment to the gold QCM surface and their effect on the quartz crystal that produces the characteristic measured Δf and ΔR shifts.

The basic observation that f decreases accompany the addition of adherent cells to the gold QCM surface has been noted previously by a number of authors (*23*−*30*). However, aside from suggesting the potential of the QCM for the study of cells, very few of these reports have attempted to systematically investigate the dependence of the Δf and ΔR shift values, produced by the addition of particular cells, on any parameters of the QCM device or differences in the cells themselves. The Sauerbray equation (eq 1) relates Δf shifts (Hz) to the elastic mass

$$\Delta f = -2\Delta m f^2/A(\mu\rho_q)^{0.5} = -C_f \Delta m \qquad (1)$$

Δm (g) bound to the crystal, where changes in f are relative to the intrinsic crystal f oscillating at 8 846 000 Hz. A is the electrode area (0.196 cm^2); ρ_q is the density of quartz (2.65 g/cm^3); μ is the shear modulus (2.95 × 10^{11} dyn/cm^2), and C_f the integrated sensitivity (0.903 Hz/ng). Many of the reports of cells binding to the QCM surface have discussed the fact that the Sauerbray equation (eq 1) does not apply to the case of cells attached to the gold QCM surface. By contrast, many inorganic systems binding to the QCM surface obey the Sauerbray eqn (*43*). This equation is applicable only to elastic masses coupled to the crystal surface, where the elastic mass can be up to a few percent (∼20 μg) of the total crystal mass. This property is why the QCM device has successfully been used to study interfacial binding phenomena. At least one protein multilayer system has been shown to obey the Sauerbray equation, acting as a purely elastic surface mass. When dried, up to 20 sequentially deposited monolayers (400 nm total thickness), composed of biotin−albumin and streptavidin on the QCM surface, obey this equation (*44*). However, when the multilayer film is hydrated, there is a 4-fold shift in the f values and the film no longer exhibits elastic mass behavior.

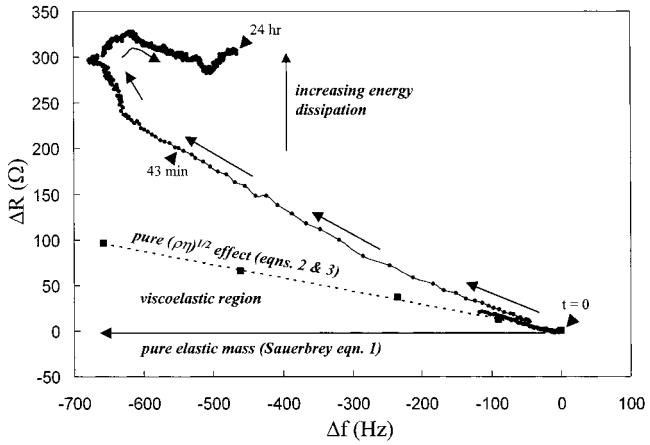

Figure 7. A Δf−ΔR diagram representation of the 30 000 added cell QCM data in Table 1. The time course of the kinetics of the Δf and ΔR values are indicated by the points starting at the origin at $t = 0$ (arrowhead) and progressing with time as indicated by the small arrows along the datapoints. The times of a few representative points are indicated (arrowheads). The Δf−ΔR points (■), determined experimentally for a series of increasing concentration sucrose solutions, are shown. The dashed line indicates the behavior of a Newtonian fluid producing a pure density−viscosity alteration of the Δf and ΔR QCM values as determined by eqs 2 and 3. QCM parameters intermediate between those of a pure bound elastic mass (horizontal line where $R = 0$) obeying the Sauerbray equation (eq 1) and a pure density−viscosity effect (obeying eqs 2 and 3) is caused by material exhibiting viscoelastic behavior. As the vertical arrow states, increasing ΔR values indicate increasing energy dissipation behavior in the solution near the solution−gold QCM surface interface.

For a pure Δf response produced by a bound elastic mass, in which the Sauerbray equation (eq 1) is obeyed, $\Delta R = 0$. Our results with attached cells clearly demonstrate that this is not the case. In all of the QCM Δf and ΔR monitoring shown in Figures 2, 3, 5, and 6 and Table 1, we observed significant ΔR shifts occurring along with Δf shifts as the cells attach, spread, and/or are stimulated to divide. One way of viewing and interpreting the relationship between these two quantities is via the Δf vs ΔR plot in Figure 7. In this case, we plotted the 24 h steady-state data from one of the kinetics experiments presented in Table 1, where 30 000 ECs were added to the QCM at time 0. At the origin of Figure 7 is the $t = 0$ point. The arrows denote the time sequence of the measured points having those particular Δf and ΔR values. For reference, a pure bound elastic mass response would be of the type shown by the horizontal arrow, where $\Delta R = 0$ for all Δf changes obeying the Sauerbray equation. Clearly the cells do not possess this type of response. A pure liquid viscosity−density change in the solution above the QCM crystal surface can also produce Δf and ΔR changes, in the absence of surface mass binding. Kanazawa et al. (*6*) was the first to derive the following equation that describes the Δf for this situation:

$$\Delta f = -f^{3/2}(\rho_L \eta/\pi\mu\rho_q)^{1/2} \qquad (2)$$

where ρ_L is the density of the liquid and η is the viscosity of the liquid. For the quartz crystal in contact with liquid, the resonant ΔR change was first derived by Muramatsu et al. (*8*):

$$\Delta R = (2\pi f \rho_L \eta)^{1/2} A/k^2 \quad (3)$$

where k is the electromechanical coupling factor. Since both Δf and ΔR are proportional to $(\rho_L \eta)^{1/2}$, the Figure 7 diagram should be a straight line for liquids of different density and viscosity. Therefore, we prepared a series of different weight percent sucrose solutions (0−46%), of varying density and viscosity, and their QCM f decrease and R increase were measured. These values are plotted as the square datapoints in Figure 7. From the known density and viscosity of these sucrose solutions, using eqs 2 and 3, Δf and ΔR values were calculated. These calculated data are presented in Figure 7 as the dashed line through the series of experimental sucrose weight percent datapoints. This dashed line indicates the behavior of a pure liquid $(\rho_L \eta)^{1/2}$ density−viscosity response. It is clear that during the time course of cells being added and attaching to the QCM surface, the increasing Δf and ΔR values they produce are changing in a manner that lies above the pure liquid density−viscosity response line.

Interpretation of data in the Figure 7 representation is as follows. For mass bound elastically to the QCM surface, producing a pure elastic mass response with $\Delta R = 0$, the horizontal line response would be observed. This represents no acoustic energy dissipation by the bound mass. In contrast, for viscoelastic materials, their ΔR values are nonzero, and they possess Figure 7 energy dissipative behaviors in the region above the elastic mass response. For certain polymeric films studied, their viscoelastic behavior places them in the energy dissipation region labeled in Figure 7, above the elastic mass response line but below the pure liquid density−viscosity response line. Examples of such polymer films are conducting polypyrrole (*8*) and micrometer-scale tubule structures composed of self-assembled decyl esters of D-tyrosine (*22*). Viscoelastic materials dissipate energy in the solution interface via a motional resistance, ΔR, as well as a Δf shift. Pure Newtonian liquids also dissipate energy through their effect on the solution interface ΔR, via density and viscosity differences as defined by eqs 2 and 3. They produce the type of Δf and ΔR responses shown by the measured sucrose solution values in Figure 7.

As we showed previously in our study of the QCM surface-bound tubules of the decyl ester of D-tyrosine, the Δf and ΔR values for the unpolymerized self- assembled micrometer-scale tubules were those characteristic of a viscoelastic material, lying in the labeled region of Figure 7. Upon enzymatic polymerization with horseradish peroxidase, during which the tubule structure did not change by SEM visualization, we observed dramatic Δf and ΔR shifts, to values approaching that of a pure liquid density−viscosity response (*22*). This shift was explained because polymerization of the self-assembled monomers in the tubule structure possibly produced density increases and certainly produced viscosity increases in the tubules that made the solution interface behave like a liquid of increased density and viscosity. As a consequence, the polymerized tubule structures dissipated more energy than the unpolymerized tubules.

We can now draw a parallel between this tubule system behavior and that of the living cells examined here, in that the internal cytoskeletal structures of the latter are also micron length dynamic structures that dissipate energy and can change those energy dissipation properties as a function of alterations in cellular state, such as the growth stimulation we study in this report. Therefore, the data reported in Figure 7 for the behavior of the ECs, being above that of the pure liquid response line, represents an even greater level of energy dissipation by the ECs in the solution interface above the QCM surface. Initially, in the first few minutes, as the spherical cells contact the surface, the time points lie closely along the pure liquid density−viscosity response line. This we interpret to be the rounded cells, absent initial surface binding contacts, altering the effective density and viscosity of the solution−gold QCM surface interface, much as a liquid would. Then, as cells spread and form surface attachments, the Δf, ΔR response with time can be seen to exhibit an increasingly negative slope. By the time of maximum cell-induced Δf shift, a state the we have demonstrated to correspond to all cells contacting and spreading on the QCM surface (*38*), the ΔR has shifted to significantly higher values (∼300 Ω), indicating increased energy dissipation by the cells. Following this point, the ΔR shift and energy dissipation level are nearly unchanged out to the steady-state 24 h value at the conclusion of the experiment. We hypothesize that this ability to dissipate energy must originate through a combination of the cellular linkages of ECs to the ECM they deposit on the QCM surface, as well as the coupling of their internal cytoskeleton to the underlying ECM via those linkages. This energy dissipative effect by the ECs represents an intriguing phenomenon that may be related to the in vivo environment of the ECs, in which these cells have evolved to respond functionally to both incoming molecular and pressure/energy signals in the pulsatile blood stream (*46*).

Trypsinization-Dependent Cell Numbers Are Responsible for Δf and ΔR Shifts. We have identified a crucial inconsistency in all of the previously published studies of cells investigated by the QCM technique. None of the previous reports determined how many cells were actually attached to the QCM surface at the conclusion of their experiments. They correlated Δf and ΔR shifts simply to the number of cells added to the QCM device. In their studies, a wide range of cell types have been used, with widely varying attachment efficiencies. As a result, a number of different complications arise in interpreting any Δf and ΔR shift data. To begin with, it was surmised but not established that attached cells and their underlying ECM were the real source of these shifts. Second, it was not possible to correlate the shift magnitudes to the cell number added.

Realizing the importance of demonstrating the dependence of the Δf and ΔR shifts on the presence of attached cells, we examined this relationship in the present report. Figure 5 and Table 1 clearly show that the trypsin 1 and trypsin 2 incubations remove the majority of the cells compared to the other washes and that this enzymatic activity is responsible for the bulk of the change in Δf and ΔR back to their pre-cell-addition values of Δf and $\Delta R = 0$.

The Δf and ΔR shift dependence on attached cells is also shown in a different way in the Table 1 counting of cells in washes from the experiment where the toxic EP O-ring was used. Here, only minor Δf or ΔR shifts were noted initially or at the steady-state time, and only a small fraction of added cells were found in the trypsin fractions. The majority of cells were found in the initial washes, indicating either that they never attached adequately and were weakly bound or that they had detached before the conclusion of the experiment.

The Table 1 trend in steady-state Δf and ΔR values with variation in either added cell number or actual attached cell number from trypsin wash counting is very minor for ΔR and is not clear for Δf. An even greater

variability for Δf was reported for VERO cells, where a constant added cell number produced a Δf shift ranging from 280 to 460 Hz (*25*). All of these results may be due to saturation of the gold surface. This saturation effect was clearly implied in another study by the plateau in Δf shifts observed with increasing numbers of added MDCK I, MDCK II, and 3T3 cells to the QCM surface (*28*). And in yet another study, there was a linear correlation between number of osteoblasts added and the % surface coverage of the crystal, determined microscopically (*24*). We are currently conducting a careful cell titration study to determine the relationship between cells requiring trypsinization to be removed from the QCM surface and the steady-state Δf and ΔR shifts observed.

Further evidence for the origin of Δf and ΔR shifts as a result of EC attachment to the gold QCM surface comes from the Figure 6 experiment. This 430 Hz drop in f following FGF addition is consistent with the estimated factor of 3.0−3.2 increase in the number of cells attached to the QCM surface using our trypsin and cell counting assay. The shift in Δf may also be due in part to a round cell phenotype. Thus, the Δf shift is likely to be caused by the significant fraction of cells possessing the round cell division phenotype and/or mitosis leading to an increase in the number of cells bound to the QCM surface.

The interpretation of these automatically recorded QCM shift values are also consistent with a proliferation assay conducted in parallel. In this parallel experiment, a standard number of cells are seeded into multichamber plates at the same initial cell density/unit surface area as existed in the QCM experiment. At 24 h following addition of cells, a number of wells were counted to establish the initial cell count, and FGF was added, at the identical concentration used in the QCM experiment, to half of the remaining wells. The growth of ECs was monitored over the next 72 h by trypsinization and electronic counting of triplicate wells containing untreated and FGF-treated cells. From these data, a growth curve, shown in Figure 6, was calculated. FGF stimulated growth by 70% compared to untreated wells. The FGF growth curve clearly parallels the relative change in Δf in the FGF stimulation experiment carried out in the QCM. These results correlate Δf shifts from the initial 0 value in the absence of cells to increasing cell numbers bound to the QCM surface. Although this fact was not entirely obvious in the added cell number Δf and ΔR trends presented in Table 1, it is clear in the Figure 6 experiment. We suspect that this is caused by a variation in the Δf and ΔR shifts between individual experiments. Currently, we are investigating the origin of the Δf and ΔR shift variability and believe it results from variation in the hydrophilic state of the gold surface. Providing a uniformly more hydrophilic gold surface through chemical pretreatment of the surface has allowed us to demonstrate consistent Δf and ΔR shifts as a function of attached cell number (*47*).

Acknowledgment

The authors acknowledge support from a Seed Grant from the Research Foundation at the University of Massachusetts Lowell and NIH grant R21 GM58583.

Accepted for publication January 25, 2000

References and Notes

(1) Sauerbray, G. Verwendung von Schwingquartzen zur Wagung dunner Schichten und zur microwagung. *Z. Phys*. **1959**, *155*, 206−222.

(2) Bruckenstein, S.; Shay, M. In situ weighing study of the mechanism for the formation of the adsorbed oxygen monolayer at a gold electrode *J. Electroanal. Chem*. **1985**, *188*, 131−136.

(3) Bruckenstein, S.; Shay, M. Experimental aspects of use of the quartz crystal microbalance in solution. *Electrochim. Acta* **1985**, *30*, 1295−1300.

(4) Kaufman, J. H.; Kanazawa, K. K.; Street, G. B. Gravimetric electrochemical voltage spectroscopy: in situ mass measurements during electrochemical doping of the conducting polymer polypyrrole. *Phys. Rev. Lett.* **1984**, *53*, 2461−2464.

(5) Nomura, T.; Watanabe, M.; West, T. S. Behavior of piezoelectric quartz crystals in solutions with application to the determination of iodide. *Anal. Chim. Acta* **1985**, *175*, 107−116.

(6) Kanazawa, K. K.; Gordon, G. The oscillation frequency of a quartz resonator in contact with a liquid. *Anal. Chim. Acta* **1985**, *175*, 99−105.

(7) Muramatsu, H.; Kimura, K. Quartz Crystal detector for microrheological study and its application to phase transition phenomena of Langmuir−Blodgett films. *Anal. Chem*. **1992**, *64*, 2502−2507.

(8) Muramatsu, H.; Egawa, A.; Ataka, T. Reliability of correlation between mass change and resonant frequency change for a viscoelastic-film-coated quartz crystal. *J. Electroanal. Chem*. **1995**, *388*, 89−92.

(9) Si, S. H.; Zhou, T.; Liu, D. Z.; Nie, L.; Yao, S. Using piezoelectric quartz crystal to study hemorheological phenomena: blood clotting and urokinase activated fibrinolysis. *Anal. Lett.* **1994**, *27*, 2027−2037.

(10) Zhou, T.; Nie, L.; Shouzhou, Y. On equivalent circuits of piezoelectric quartz crystals in a liquid and liquid properties. *J. Electroanal. Chem*. **1990**, *293*, 1−18.

(11) Fawcett, N.; Evans, J. A.; Chien, L.; Flowers, N. Nucleic acid hybridization detected by piezoelectric resonance. *Anal. Lett.* **1988**, *21*, 1099−1114.

(12) Su, H.; Yang, M.; Kallury, K. M. R.; Thompson, M. Interfacial nucleic acid hybridization studied by random primer 32P labeling and liquid-phase acoustic network analysis. *Anal. Chem*. **1994**, *66*, 769−777.

(13) Su, H.; WIlliams, P.; Thompson, M. Platinum anticancer drug binding to DNA detected by thickness shear mode acoustic wave sensor. *Anal. Chem*. **1995**, *67*, 1010−1013.

(14) Ito, K.; Hashimoto, K.; Ishimori, Y. Quantitative analysis for solid-phase hybridization reaction and binding reaction of DNA binder to hybrids using a quartz crystal microbalance. *Anal. Chim. Acta* **1996**, *327*, 29−35.

(15) Muratsugu, M.; Kurosawa, S.; Kamo, N. Detection of antistreptolysin O antibody: application of an initial rate method of latex piezoelectric immunoassay. *Anal. Chem*. **1992**, *64*, 2483−2487.

(16) Ghouechian, H. O.; Kamo, N.; Hosokawa, T.; Akitaya, T. Improvement of latex piezoelectric immunoassay: detection of rheumatoid factor. *Talanta* **1994**, *41*, 401−406.

(17) Thompson, M.; Arthur, G. L.; Dhaliwal, G. K. Liquid-phase piezoelectric and acoustic transmission studies of interfacial immunochemistry. *Anal. Chem*. **1986**, *58*, 1206−1209.

(18) Chang, H. C.; Yang, C. C.; Yeh, T. M. Detection of lipopolysaccharide binding peptides by the use of a lipopolysaccharide coated piezoelectric crystal biosensor. *Anal. Chim. Acta* **1997**, *340*, 49−54.

(19) Fukuoka, S.; Karube, I. Influence of cationic antibiotics on phase behavior of rough form lipopolysaccharide. *Appl. Biochem. Biotechnol.* **1994**, *49*, 1−9.

(20) Rickert, J.; Weiss, T.; Kraas, W.; Jung, G.; Gopel, W. A new affinity biosensor: self-assembled thiols as selective monolayer coatings of quartz crystal microbalances. *Biosens. Bioelectron.* **1996**, *11*, 591−598.

(21) Imai, S.; Mizuno, H.; Suzuki, M.; Takeuchi, T.; Tamiya, E.; Mashige, F.; Ohkubo, A.; Karube, I. Total urinary protein sensor based on a piezoelectric quartz crystal. *Anal. Chim. Acta* **1994,** *292*, 65−70.

(22) Marx, K. A.; Zhou, T.; Sarma, R., Quartz crystal microbalance measurement of self-assembled micellar tubules of the amphiphilic decyl ester of D-tyrosine and their enzymatic polymerization. *Biotechnol. Prog.* **1999**, *15*, 522−528.
(23) Matsuda, T.; Kishida, A.; Ebato, H.; Okahata, Y., Novel instrumentation monitoring in situ platelet adhesivity with a quartz crystal microbalance. *ASAIO J.* **1992**, *38*, 171−173.
(24) Redepenning, J.; Schlesinger, T. K.; Mechalke, E. J.; Puleo, D. A.; Bizios, R. Osteoblast attachment monitored with a quartz crystal microbalance. *Anal. Chem.* **1993**, *65*, 3378−3381.
(25) Gryte, D. M.; Ward, M. D.; Hu, W. S., Real time measurement of anchorage dependent cell adhesion using the quartz crystal microbalance. *Biotechnol. Prog.* **1993**, *9*, 105−108.
(26) Nivens, D. E.; Chambers, J. Q.; Anderson, T. R.; White, D. C. Long-term on-line monitoring of microbial biofilms using a quartz crystal microbalance. *Anal. Chem.* **1993**, *65*, 65−69.
(27) Muratsugu, M.; Romanschin, A. D.; Thompson, M. Adhesion of human platelets to collagen detected by Cr51 labeling and acoustic wave sensor. *Anal. Chim. Acta* **1997**, *342*, 23−29.
(28) Wegener, J.; Janshoff, A.; Galla, H. J. Cell adhesion monitoring using a quartz crystal microbalance: comparative analysis of different mammalian cells lines. *Eur. Biophys. J.* **1998**, *28*, 26−37.
(29) Fredriksson, C.; Kihlman, S., Rodahl, M.; Kasemo, B. The piezoelectric quartz crystal mass and dissipation sensor: a means of studying cell adhesion. *Langmuir* **1998**, *14*, 248−251.
(30) Fredriksson, C.; Kihlman, S.; Rodahl, M.; Kasemo, B. In vitro real-time characterization of cell attachment and spreading. *J. Mater. Sci.: Mater. Med.* **1998**, *9*, 785−788.
(31) Nicosia, R. F.; Villaschi, S. Autoregulation of angiogenesis by cells of the vessel wall. *Int. Rev. Cytol.* **1999**, *185*, 1−43.
(32) Hungerford, J. E.; Little, C. D. Developmental biology of the vascular smooth muscle cell: building a multilayered vessel wall. *J. Vasc. Res.* **1999**, *36*, 2−27.
(33) Michel, C. C.; Curry, F. E. Microvascular permeability. *Physiol. Rev.* **1999**, *79*, 703−761.
(34) Engerman, R. L., Pfaffenbach, M. D., Davis, M. D. Cell turnover of capillaries. *Lab. Invest.* **1967**, *17*, 738−741.
(35) Weidner, N.; Semple, J. P., Welch, W. R.; Folkman, J. Tumor angiogenesis and metastasis-correlation in invasive breast carcinoma. *N. Engl. J. Med.* **1991**, *324*, 1−8.
(36) Barakat, A. I. Responsiveness of vascular endothelium to shear stress: potential role of ion channels and cellular cytoskeleton (review). *Int. J. Mol. Med.* **1999**, *4*, 323−332.
(37) Ingber, D. E. Tensegrity: the architectural basis of cellular mechanotransduction. *Annu. Rev. Physiol.* **1997**, *59*, 575−599.
(38) Zhou, T.; Braunhut, S. J.; Medeiros, D.; Marx, K. A. Cellular adhesion and spreading of endothelial cells monitored in real time using the quartz crystal microbalance. *Tissue Eng. Sym.: Mat. Res. Soc.* **1999**, *550*, 177−182.
(39) Braunhut, S. J.; Palomares, M., Modulation of endothelial cell shape and growth by retinoids. *Microvasc. Res.* **1991**, *41*, 47−62.
(40) Martin, B. A.; Hager, H. E. Flow profile above a quartz crystal vibrating in liquid. *J. Appl. Phys.* **1989**, *65*, 2627−2629.
(41) Martin, B. A.; Hager, H. E. Velocity profile on quartz crystals oscillating in liquids. *J. Appl. Phys.* **1989**, *65*, 2630−2635.
(42) Lin, Z.; Ward, M. D. The role of longitudinal waves in quartz crystal microbalance applications in liquids. *Anal. Chem.* **1995**, *67*, 685−693.
(43) Ward, M. D. Principles and applications of the electrochemical quartz crystal microbalance. In *Physical Electrochemistry: Principles, Methods and Applications*; Rubenstein, I., Ed.; Marcel Dekker: New York, NY, 1995; pp 293−338.
(44) Rickert, J.; Brecht, A.; Gopel, W. QCM operation in liquids: constant sensitivity during formation of extended protein multilayers by affinity. *Anal. Chem.* **1997**, *69*, 1441−1448.
(45) Muramatsu, H.; Tamiya, E.; Karube, I. Computation of equivalent circuit parameters of quartz crystals in contact with liquids and study of liquid properties. *Anal. Chem.* **1988**, *60*, 2142−2150.
(46) Papadaki, M.; Eskin, S. G. Effects of fluid shear stress on gene regulation of vascular cells. *Biotechnol. Prog.* **1997**, *13*, 209−221.
(47) Zhou, T.; Marx, K. A.; Warren, M.; Braunhut. S. Hydrophilic surface Modification of the quartz crystal microbalance improves endothelial cell adhesion and spreading, manuscript in preparation.

BP000003F